www.ietdl.org

Published in IET Generation, Transmission & Distribution
Received on 1st April 2014
Revised on 24th October 2014
Accepted on 2nd November 2014
doi: 10.1049/iet-gtd.2014.0287

Special Issue on Sensors and Data Analytics for Smart Grid Infrastructure

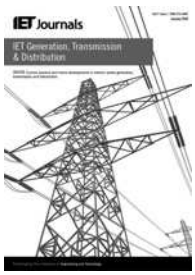

ISSN 1751-8687

Data analytics based neuro-fuzzy controller for diesel-photovoltaic hybrid AC microgrid

P.C. Sekhar[1], *Sukumar Mishra*[2], *Rishi Sharma*[2]

[1]*Department of Electrical Engineering, National Institute of Technology Warangal, India*
[2]*Department of Electrical Engineering, Indian Institute of Technology Delhi, New Delhi, India*
E-mail: psekhar.chandra@gmail.com

Abstract: The diesel-photovoltaic (PV) based hybrid AC microgrid systems with conventional control philosophies deliver very good performance in the grid connected mode. However, once the microgrid is isolated from the main grid the same philosophies which control the PV at its maximum power can make the microgrid unstable. In this connection, this study proposes a novel neuro-fuzzy controller to ensure the smooth transition of microgrid from grid connected mode to isolated mode, to retain the system stability even in isolated mode and to deliver the superior performance in grid connected mode as well. The considered artificial neural networks is trained with P_{MPP}–Temp against V_{MPP} characteristic, first of its kind. The fuzzy part of the controller derives the reference voltages subjected to the limits provided by the ANN. This study describes how well the data analytics can be utilised to retain the power system stability in emergencies. The proposed controller has been evaluated under different operating conditions and is exhibiting superior performance in achieving the desired control objectives. Results from the numerical simulations are confirmed from the experiments in real-time environment.

1 Introduction

The main objective of smart grid is to ensure uninterrupted, quality power supply to the needy consumers at reduced cost without violating environmental constraints. In order to meet this objective, an effective utilisation of environment friendly power resources, like photovoltaic (PV), fuel cell and wind based energy generations, is required. However, the goals of smart grid can only be met through proper coordination of all these resources along with the existing conventional generations like diesel engine driven synchronous generators (DEG), hydro and thermal generators. Data analytics plays a very vital role in smart grid management, as most of the control decisions for the coordination of different devices are made based on the conclusions drawn from the available data. In [1], authors outlined the significant role of data analytics that can play in maintaining the system stability. It is anticipated that the smart grid generates huge amounts of high-velocity data through efficient communication technologies because of the deployment of smart meters, phasor measurement units and other protection devices for efficient, reliable and secured operation of the system. Hence, it is high time to design the decision making systems with minimum data acquisition and processing requirements. In this connection, this paper considers one of such problems where the amount of data to be collected and processed can be reduced without compromising on system efficiency, reliability, security and proposes a novel control philosophy for the effective management of DEG-PV based microgrid system in both grid connected and off-grid modes.

Distributed generators which form the microgrid, operate generally in a grid connected mode, however, circumstances such as fault, voltage sag and other disturbances in the main grid or may be because of geographical limitations microgrids are disconnected from the main grid and forced to operate as an 'isolated microgrid' [2]. To operate the synchronous machine in synchronism with the other sources and to obtain the desirable performance from the apparatus, the frequency of operation should be maintained within a stipulated band. The control strategies discussed in the literature [3] can render very good performance in obtaining a power balance, if the microgrid is in grid connected mode. However, in isolated mode, regulation of frequency following a disturbance is more challenging because of the limited availability of energy resources, inertia and loads. Since, most of the today's hybrid microgrid installations employs DEG and PV generators as sources and the DEG-PV based hybrid systems have been demonstrated as reliable, feasible and environmentally friendly solution to supply energy demand in remote locations [4], this study concentrates on the frequency control of a microgrid with these generators as sources in both grid connected and isolated modes. In general, the DEG supplies at least a minimum power to the system to prevent its mechanical damage. A typical but highly probable load scenario of DEG-PV based microgrid is its generation greater than the load. This condition may arise either because of islanding of microgrid from the main grid or because of change in generation or loading conditions in an islanded microgrid. If the grid connection is available, the PV is controlled at its maximum power point [5], and the excess power is

supplied to the grid. However, when the grid is unavailable, the excess power will be fed to the DEG resulting in reversal of power flow, and hence undergo motoring mode. Therefore the speed of the DEG will continue increasing even if there a governor in the loop. Since, the speed of the DEG decides the microgrid frequency, it will rise to abnormal values and the system loses its stability [6]. Besides, the excess power not only affects the system frequency, it results in increase of voltage magnitude, poor power quality leading to reduction in life time of other devices along with the DEG [7]. By a proper control mechanism the excess power can be diverted to storages or dump loads [8]. For example, a microgrid controlled by PI regulators is studied in [9], and by a PSO based fuzzy controller is considered in [10] with flywheel and battery as reserves for providing frequency control services. However, they involve high initial and operational costs [11, 12]. Therefore a special control mechanism to retain the stability of an isolated microgrid under all operating conditions without any extra storage or dump loads is highly essential.

A PV-Diesel hybrid system is examined in [4], however the microgrid transition from grid connected mode to isolated mode in which the possibility of aforementioned case of more generation than the load is not considered. Even though the isolated PV-Diesel systems are analysed in [13–15], the operational complexities under emergency conditions are not adequately explored. For this, an effort has been made in [7], however the proposed control methodology follows the look-up table based approach and requires insolation measurement, hence demanding extra, costly sensing hardware. Apart from extra cost, the decision making based on insolation measurement is not preferable, since the spectral sensitivities of pyranometer and the PV panel may not be the same, resulting in inaccurate control decisions. To overcome these limitations, a PI based control decision approach is proposed in [16]. Since it uses perturb and observe (P&O) based approach, the system may become unstable for ramp change of insolations. The control decisions are adopted using PI controller, resulting in poorer adaptive control [17], especially in emergency conditions. Therefore a novel control methodology to regulate the frequency of a DEG-PV based hybrid AC microgrid both in grid connected and isolated modes thereby ensuring stable operation of the system under all possible operating conditions is proposed in this paper. The suggested methodology controls the DEG-PV microgrid with the help of a novel neuro-fuzzy controller and it does not require any extra storage, dump load, insolation sensor. The proposed methodology depicts how well the data acquisitions based control algorithms can be employed to handle the typical stability problems expected to encounter in upcoming renewable rich smart grids.

In this paper, Section 2 gives a brief idea of the considered hybrid microgrid and its control schematic. Limitations of the conventional controllers are discussed in Section 3. The analysis of P&O based approaches is given in Section 4. Section 5 describes the ANN based tracker developed based on data analytics and its design procedure. Section 6 discusses the proposed neuro-fuzzy controller in detail. The proposed control philosophy is validated in Section 7 under different generation and loading conditions, in grid connected and isolated modes. Section 8 compares the performance of the proposed controller with the existing controllers. Section 9 confirms the superior performance of the proposed control philosophy through experimental results in real-time environment. This paper is concluded in Section 10.

2 DEG-PV based hybrid AC microgrid

The considered hybrid microgrid comprises of a diesel driven generator and an electronically coupled PV generator as shown in Fig. 1*a*. The variable loads are considered to be an induction motor and impedance loads. This microgrid is connected to the main grid at PCC through a step-up transformer and a distribution feeder. Modelling of the different generators is briefly discussed in this section, whereas the control philosophy and its associated different controllers are discussed in the succeeding sections.

2.1 PV generator

The PV generator is a photosensitive device and can be modelled with a current source representing the photo current (I_{ph}), a diode, a series resistance to account for internal resistance to the current flow and a parallel resistance to consider the leakage current. The PV model has been developed with reference to [18–20] in this paper. The power output of any PV array holds non-linear relationship with its voltage and will increase with increase in insolation and decreases with rise in temperature as shown in Fig. 1*b* in which 100% of insolation corresponds to 1000 W/m^2.

Voltage source converters (VSCs) play a very vital role in the grid integration of renewable energy based sources, like PV, fuel cells and wind generators [21, 22], as they can ensure black start and fast restoration in case of complete grid collapse. VSCs with proper control philosophy can have decoupled real and reactive power control which is of great importance in maintaining the system voltage or power factor without affecting the real power flow [23–25]. Further, the frequency control can be appropriately introduced to maintain the system stability under islanding scenarios and help the system in tiding over disturbances [26]. VSCs allow asynchronous interconnection which is helpful in isolating the grid disturbances from entering the healthy system. This feature of VSC has resulted in back-back HVDC links and FACTS concepts. In view of the aforementioned advantages, VSC has become a first choice converter for grid integration of renewable energy sources and hence it is used in this paper to integrate the PV generator with the grid.

2.2 Diesel engine driven synchronous generator

For many years, DEGs are the first to be used in distributed generation technologies because of their reliability in both the grid connected and off grid operations. In order to meet the change in the load demands/generation, the power output from engine and hence the generator has to be varied as indicated in Fig. 1*a*. The governor of the diesel engine adjusts the fuel input to the engine via a valve mechanism thereby regulating the input of the engine which further regulates the generator output power, finally provides the required power to meet the changes in the load demand. As the DEG modelling is well accomplished in many literatures, it is not discussed in this paper.

3 System performance with conventional controllers

In a hybrid system, with the conventional control philosophy as suggested in many literatures [3], all the weather dependent

doi: 10.1049/iet-gtd.2014.0287

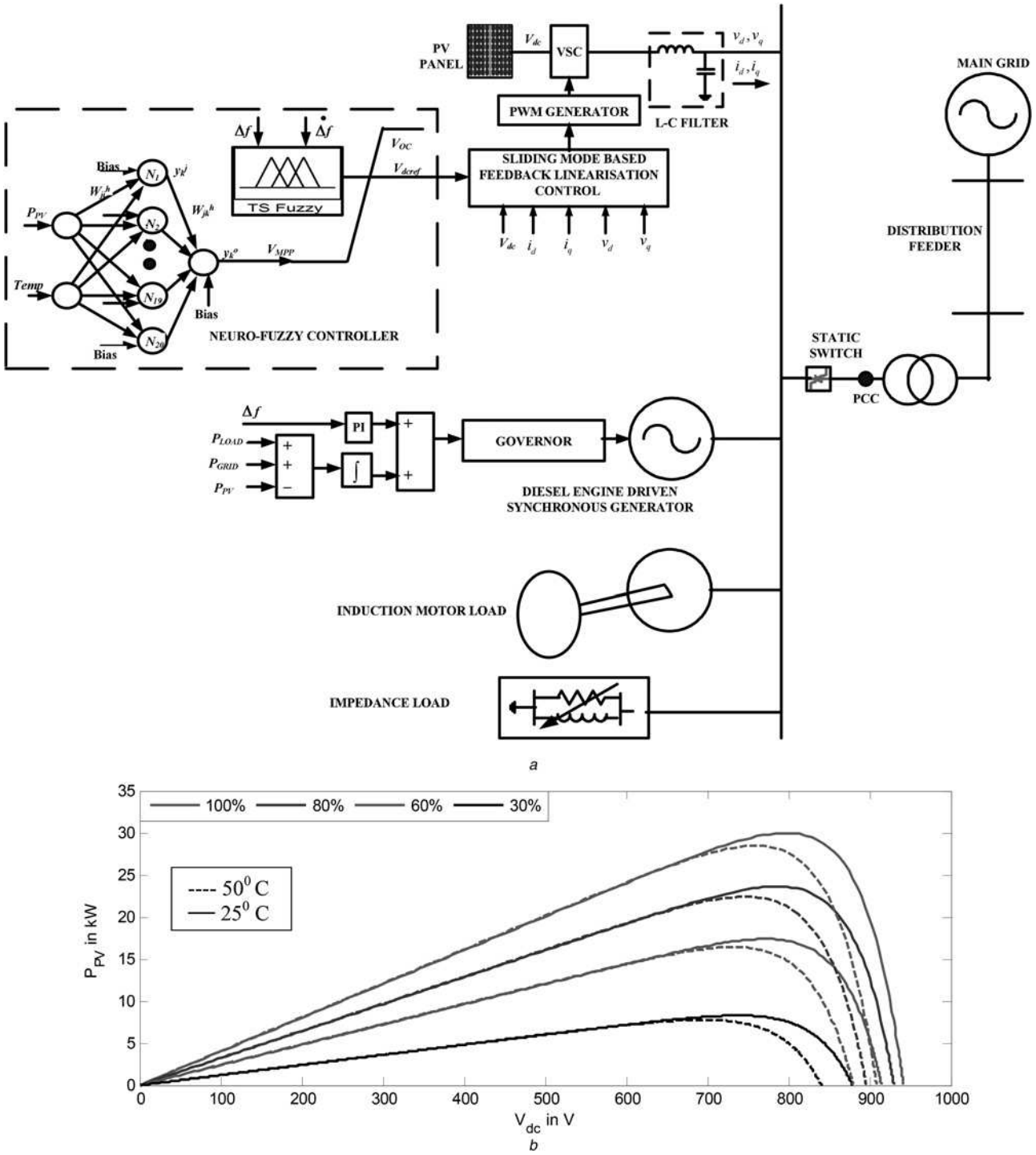

Fig. 1 *DEG-PV based hybrid AC Microgrid*

a Schematic diagram of DEG-PV hybrid AC microgrid
b Variation of the PV generator power and MPP with insolation and temperature changes

renewable energy sources like PV and wind are controlled to deliver maximum available power to the system, either to utilise the renewable sources to maximum extent thereby reducing their unit costs or to reduce the carbon foot print or may be both. However, it may not be feasible in all the cases. For example, Fig. 2*a* shows the power flows in a conventionally controlled DEG-PV based hybrid microgrid (Fig. 1*a*) which is assumed to be isolated from the grid at 3 s. The DEG is generating a power of 15 kW prior to the isolation. With the conventional control strategy, the PV generator is operated at MPP, all the time, and is delivering 30 kW as depicted in Fig. 2*a*. The total load on the system, which includes the induction motor and impedance load, is 20 kW. Therefore, prior to the isolation, microgrid is supplying the power to the tune of 25 kW (30 kW + 15 kW – 20 kW) to the main grid as shown in Fig. 2*a*. Owing to the losses incurred in the system, the actual grid feeding is a little less than 25 kW as shown in Fig. 2*a*. Once the microgrid is isolated from the main grid at 3 s, the available generation in the microgrid becomes excess to the load. Hence, this surplus power flows into the DEG resulting in reverse flow of power that is from positive power to the

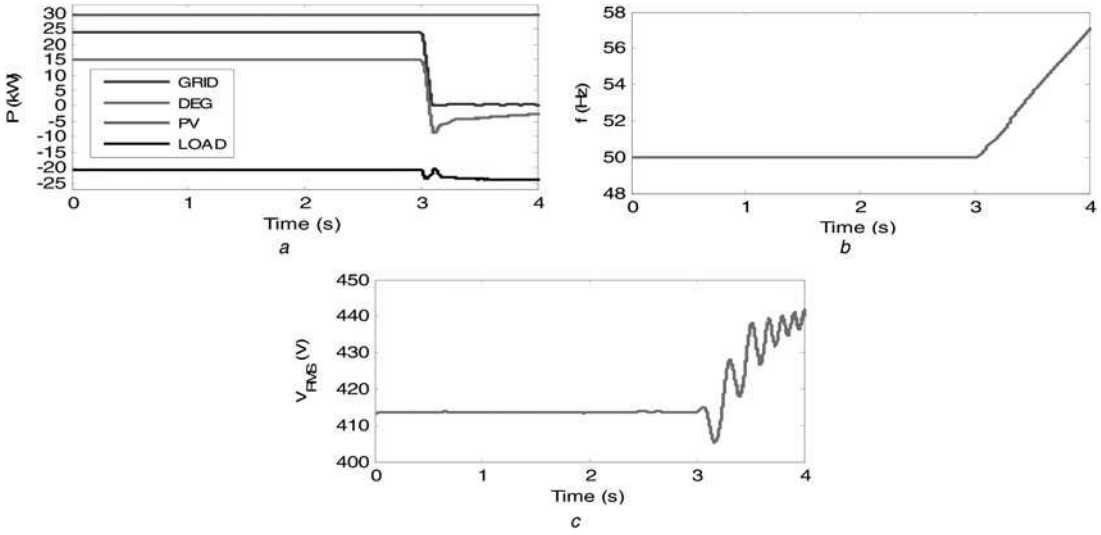

Fig. 2 *Performance with conventional control philosophy*

a Power flows from different generators and to the loads, grid
b System frequency
c Terminal voltage

negative power as shown in Fig. 2*a*. This forces the DEG to run as motor and hence the frequency starts rising to dangerous levels as depicted in Fig. 2*b*, thereby system loses its stability. During this process, the system voltage also gets influenced to a large extent both in terms of frequency and magnitude as shown in Fig. 2*c*. All these consequences result in damage of all the associated equipments including the generators. This kind of situation may arise not only during the transition from the grid connected mode to isolated mode, even in an isolated microgrid with insolation and/or load changes as well.

From Fig. 2 it can be concluded that the conventional control philosophies are not feasible for all the operating conditions in a DEG-PV based hybrid AC microgrid. Hence there is a necessity to develop a control methodology which can assure the system stability in all possible operating conditions.

4 Analysis with P&O based controllers

To address the problem discussed in the Section 3, a solution has been proposed in [7]; however, its main limitation is necessity of load power calculation which may not be readily available. It also follows the look-up table based approach which requires insolation measurement. Hence, authors in [16] proposed novel methodology using P&O based approach and the PV generator is controlled by a PI

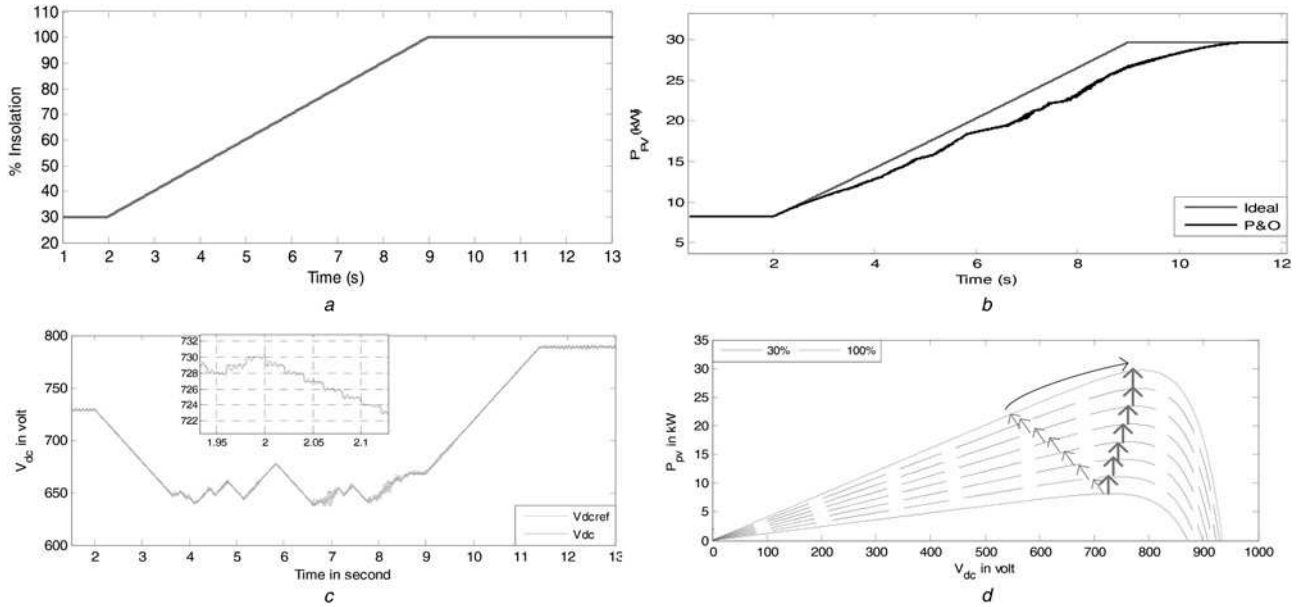

Fig. 3 *Performance with P&O based trackers for ramp insolation changes*

a Insolation change
b PV power
c PV voltage
d Confusion of P&O based tracker for ramp insolation change

doi: 10.1049/iet-gtd.2014.0287

controller. Since the methodology follows a P&O based approach, the limitations arising from the inherent procedure that the P&O adapts will affect the system performance and can make the system unstable. A case study is presented here in this section to ascertain the same.

A ramp or slow insolation change of 10%/second from 30 to 100%, starting at 2 s, is considered as shown in Fig. 3*a* and the corresponding MPP is tracked with the P&O based tracker whose performance is as shown in Figs. 3*b* and *c*. The P&O based trackers take the perturb decision based on the change in power output with the perturbation. As it is seen from Fig. 3*a*, the insolation starts rising from 2 s, however the P&O cannot differentiate between the power changes because of the perturbations from that of the power changes because of isolation changes. Hence, it misreads the increase in power output as it is because of the perturbation and not because of the insolation change. As depicted in Fig. 3*c*, the perturbation generated by the P&O has happened to be negative which prompts the P&O to further generate the negative perturbation and hence decrease of the PV voltage. This trend of generating negative perturbations and decrease of voltage will continue as shown in Figs. 3*c* and *d*, till the insolation becomes steady or the change is negligible, so that the net change in power reflects the perturbation change. During the course of perturbations, the P&O may generate either positive perturbs or negative perturbations, irrespective of the insolation change but depending on the net change in power output for the last perturbation. With this confusion, P&O delivers a highly oscillating power resulting in inconsistency in the PV output, thereby affecting the entire system and can make the system unstable.

From Fig. 3, it can be concluded that the P&O based control philosophies used for the control of DEG-PV based hybrid microgrid are more prone to instability during the ramp insolation changes which is unavoidable in real world.

From the above discussion it can be deduced that the P&O based control philosophies are delivering substandard performance because of its inherent procedure of output power slope dependent perturb decisions. In this connection, a novel mechanism is developed to make the tracking performance independent of the slope of PV outputs without using any extra sensors and with minimum data handling requirement. The developed control algorithm makes use of adaptive capability of artificial neural networks (ANN) in decision making. The considered ANN is trained with a data derived from novel but simple procedures, thereby delivering more stable performance under all operating conditions.

5 ANN based MPP tracker

As aforementioned, the P-V characteristics will vary with insolation and temperature. However, for every set of insolation and temperature P-V characteristic of any module is unique. Hence, the ANN has been trained with voltage, current and temperature as inputs, to predict the V_{MPP} in [27]. This procedure demands huge data sets and networks size will be large (total 4279 data sets are used to train the ANN with 300 hidden neurons in [27]). Owing to the requirements of large data sets and involved complexity of ANN, the training will be rigorous and time consuming. Another limitation of these methodologies is that their implementation can only be carried out through high performance microcontrollers. In order to eliminate the identified disadvantage of P&O based mechanisms and limitations of existing ANN based mechanisms, this paper considers a novel mechanism as explained in this section.

For each set of insolation and temperature, the operating voltage at which the module is to be operated to extract the maximum power P_{PVMAX} is unique. Hence, these unique operating voltages (V_{MPPs}) for different sets of insolation and temperature are determined by controlling the DC link voltage using a capacitor charging and discharging circuits. It can also be done through external loading circuits. A curve (thick black line(s) in Fig. 4*a*) can be developed with this data of V_{MPP} and P_{PVMAX} which depicts the relation between the output power and the DC link voltage of the PV panel for maximum power extraction at that particular temperature. On the other hand, this curve simply characterises the behaviour of PV panel for maximum power extraction. In order to have an accurate tracker with the best tracking capabilities, it is advisable to subject the

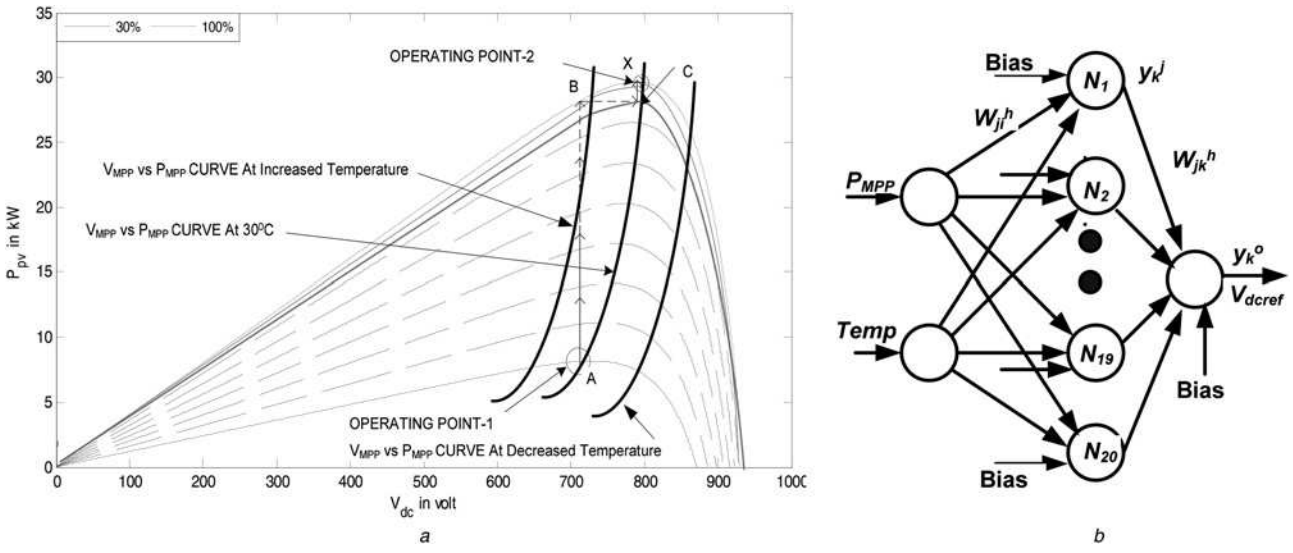

Fig. 4 *ANN based MPP tracker*

a Characterisation of PV module for extraction of maximum power under different insolations and temperatures
b Feedforward ANN considered for P_{MPP}–Temp against V_{MPP} characteristic training

PV panel to as many different insolations and temperatures as possible. A characteristic equation which involves the polynomial coefficients can be developed that fits best to the 'P_{PVMAX} against V_{MPP}' curve as given in (1)

$$V_{MPP} = \sum_{(i=1,j=x)}^{(i=x+1,j=0)} C_i P^j \tag{1}$$

where, C_i denotes the polynomial coefficients and P^j denotes the P_{PVMAX}. The number of coefficients (C_i) depends on the order of the curve equation that fits best. For example a fitting function with sixth order polynomial can be written as:

$$V_{MPP} = C_1P^6 + C_2P^5 + C_3P^4 + C_4P^3 + C_5P^2 + C_6P^1 + C_7 \tag{2}$$

5.1 Tracking principle

Assume the insolation as 300 W/m^2, prior to the change, and is increased to 1000 W/m^2 (i.e. from 30 to 100%) during the operation. Let the operation is at operating point-1 (A) prior to insolation change as shown in Fig. 4*a* which is the MPP for 30% insolation. With the change in insolation from 30% to 100%, the operation will be shifted to *B* which corresponds to the same V_{MPP} of 30% insolation but on the PV characteristic of 100% insolation (top most characteristic), results in increased power output. However, this new power corresponds to another voltage on the 'P_{MPP} against V_{MPP}' curve, that is, it would be the maximum power output for some other insolation. Since the system is instructed to track the 'P_{MPP} against V_{MPP}' curve, the module is given with a reference voltage that corresponds to *C*. By this, the operation will be shifted to *X* on the 100% insolation characteristic, however with the voltage corresponding the operating point *C*. This indirectly generates a large perturbation. Corresponding to this new voltage reference, there will be another power output for the changed insolation (1000 W/m^2). Owing to the new power output, the 'P_{MPP} against V_{MPP}' curve further generates a different reference voltage thereby generating another perturbation, however less than the earlier perturbation. Likewise, the tracking system keeps on predicting the new reference voltages by following 'P_{MPP} against V_{MPP}' curve till the new MPP (operating point-2) is reached. This results in quick and accurate tracking of MPP in a very few adaptive perturbations (ΔV_{dc}) as given in (3)

$$\left.\begin{aligned} V_{dcref}(n+1) &= f\left(P_{PVMAX}\text{versus}V_{MPP}\right)\big|_{T_c = 30^o\text{and}\ P_{PVMAX}=P_{PVMAX}(n)} \\ V_{dcref}(n+1) &= V_{dc}(n) + \Delta V_{dc}(n) \end{aligned}\right\} \tag{3}$$

As the operation moves towards the MPP, perturbations become smaller and will be zero on reaching the MPP. Summarising the above discussion, the proposed tracker predicts the V_{MPP} through adaptive perturbations and the error in the predicted V_{MPP} will be corrected by following the 'P_{MPP} against V_{MPP}' curve. However, the characteristic equation, and hence the 'P_{MPP} against V_{MPP}' curve, is unique for every temperature as shown in Fig. 4*a*. Therefore, a single polynomial curve is insufficient to accurately predict the optimal operating point for varying temperatures even with same insolation, which is the practical case scenario in different seasons of a year. Hence for accurate prediction of V_{MPP}, consideration of number of polynomial characteristics, one for each operating temperature, is mandatory. However, it is not practically feasible to get the characteristics for each and every operating temperature under different insolations. This necessitates the non-linear mapping of 'P_{MPP} against V_{MPP}' characteristics against different temperatures that is 'P_{MPP}–Temp against V_{MPP}'. Hence, a feedforward ANN is considered in this study as shown in Fig. 4*b*. The considered ANN is trained with back propagation algorithm for the P_{MPP}–Temp against V_{MPP} characteristic at different insolations and temperatures to adapt the perturbations, thereby realising a 'ANN based adaptive-predictor-corrector' tracking mechanism.

The inputs in the proposed tracker are only two, PV power output P_{pv}, temperature and the output is V_{dcref}. The training sets have been considered with 20 insolation changes, each of 5%, from 50 W/m^2 to 1000 W/m^2 and 6 temperature changes, each of 10°C, from 10°C to 60°C. Hence, total 120 training sets, with total 360 (120 * 3, (two inputs and one output)) elements, are considered to train the ANN. The ANN consists of single hidden layer with 20 hidden neurons is considered in this study. The model structure with respect to number of hidden neurons is decided by using the five-fold cross validation technique and it is finally determined that ANN with 20 hidden neurons is the best performing structure for the testing data set. Hence, the ANN used in this study consists of one hidden layer having 20 neurons, two neurons in the input layer and a single neuron in the output layer to predict the MPP voltage. As shown in Fig. 4*b*, P_{PV} and Temp are the inputs and V_{dcref} is the output of ANN at which the PV module needs to be operated for maximum power extraction. The ANN is trained with Levenberg–Marquardt back propagation methodology, hyperbolic tangent sigmoid transfer function (TANSIG) is chosen as the activation function with mean square error as the cost function. From the data set, 70, 15 and 15% of the data has been used for the training, validation and testing purposes, respectively.

6 Proposed neuro-fuzzy controller

When the microgrid is operating in grid connected mode, the PV generator is controlled to deliver maximum power and the DEG is controlled to generate scheduled power subjected to its minimum operating load (P_{DEGmin}). However, once the microgrid is isolated from the main grid, proper coordination among the DEG-PV is necessary to maintain the system stability, as concluded in Section 3. When the load is greater than the power that can be extracted from the PV (P_{PVmax}) and the P_{DEGmin}, the DEG is regulated to deliver the balance power to the load. However, during the scenarios where the load is less than the P_{PVmax} plus the P_{DEGmin}, the system will become unstable in isolated mode, unless a proper control action is initiated. In this scenario the only control option available is to regulate the PV below its maximum power thereby ensuring the energy balance and hence the stability.

In the proposed philosophy, the controller keeps on tracking the microgrid frequency. If the microgrid is operating in grid connected mode, the objective of the controller is to deliver the maximum possible power from

doi: 10.1049/iet-gtd.2014.0287

the PV and to regulate the DEG according the set point as the frequency is maintained by the main grid. Once the microgrid gets isolated from the main grid, the DEG tries to come to its P_{DEGmin} to ensure maximum utilisation of PV power. The DEG starts responding only when the load is greater than the P_{PVmax} plus the P_{DEGmin}, otherwise it delivers only P_{DEGmin}. When the load is less than the P_{PVmax} plus the P_{DEGmin}, the system starts entering the unstable region which will be indicated through rise. In microgrid frequency. Since the DEG is already operating at its minimum loading capacity, the PV has to be regulated. In fact, it has to be controlled to deliver less power than its maximum possible power which is accomplished through a neuro-fuzzy controller as shown in Fig. 1*a*.

Whenever the PV is delivering the power output other than its maximum possible value for the existing operating conditions, there are two operating points, say A and B on the two sides of MPP as shown in Fig. 5. Operation at point A is characterised by low voltage, whereas operation at point B is characterised by high voltage for the same power output. Since the operation at point B results in less modulation index for the same interconnection voltage, the VSC which is used to interface the PV to the system will not enter the non-linear operating region. By maintaining the VSC in linear operating region, one can avoid the possibility of losing control over the power delivered to the system and hence the system stability. Therefore, the controller is designed to derive reference voltages which are higher than the V_{MPP} based on the frequency deviation and its rate.

Fuzzy controller for PV generation control: The ANN in the controller generates the V_{dcref} as explained in Section 5. The fuzzy controller derives the required change in operating voltage ΔV_{dcFCS} such that the operating voltage is limited by the V_{MPP} on the lower side, where as the upper limit is decided by the open circuit voltage at which the PV power output is zero as shown in Fig. 1*a*. Inputs to the fuzzy controller are change in frequency Δf and rate of change in frequency $\dot{\Delta f}$. These inputs, which are classified into five different classes as large positive (LP), small positive (SP), zero (Z), small negative (SN) and large negative (LN) as shown in Fig. 5*b*, are passed through the rule base after the normalisation. The rule base which decides the ΔV_{dcFCS}, hence the ΔP_{PV}, is given in Table 1. For the output (ΔV_{dcFCS}), membership values are chosen as 65, 35, 0, −35 and 65, respectively, from LP to LN. All the above parameters are given in the appendix. Weighted average method is used to determine the final output ΔV_{dcFCS} after de-normalising the fuzzy output. The VSC of PV generator is controlled by a non-linear controller known as feedback linearised sliding mode controller (FBLSMC) to attain the set point quickly and accurately. Control of VSC, design of FBLSMC and its stability related issues are

Table 1 Fuzzy rule base

$\dot{\Delta f}$ / Δf	LP	SP	Z	SN	LN
LP	LP	LP	SP	Z	Z
SP	LP	SP	SP	Z	Z
Z	SP	SP	Z	Z	SN
SN	Z	Z	SN	LN	LN
LN	Z	SN	SN	LN	LN

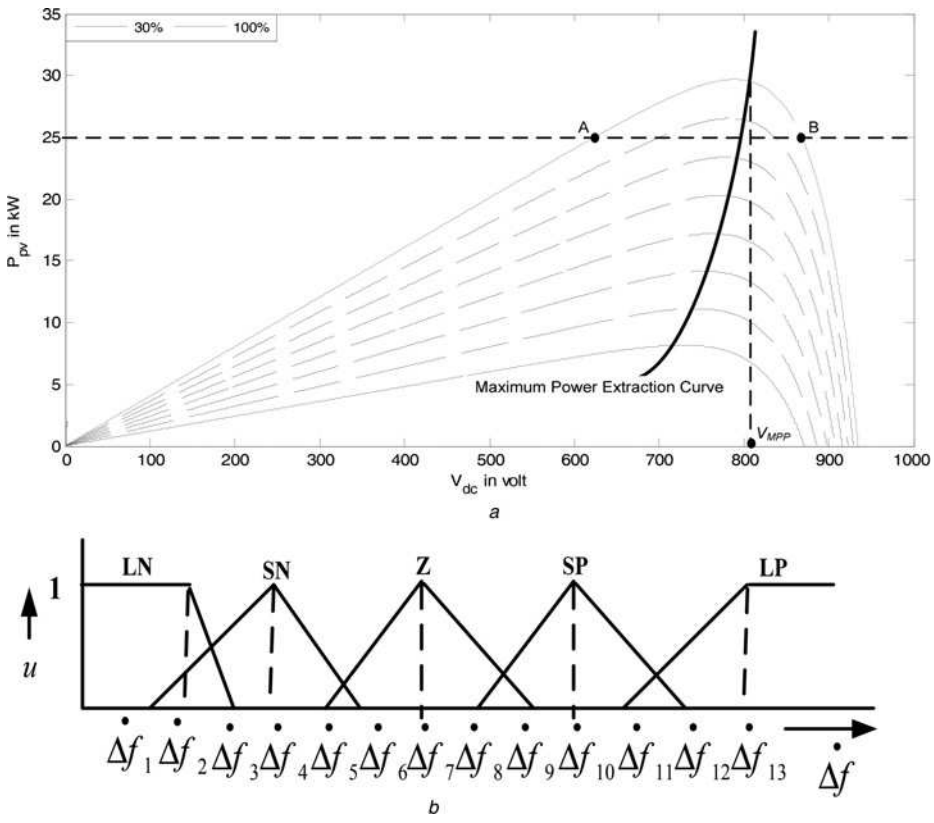

Fig. 5 *Operation of proposed neuro-fuzzy controller*

a Controlling the PV Generator at operating point other than its MPP
b Distribution of input over different classes

not discussed in this paper because of word limit constraint; interested readers may please refer to [28].

7 Performance analysis with proposed neuro-fuzzy controller

In order to test the efficacy of proposed neuro-fuzzy controller, all the possible operating, generation and loading scenarios are considered in this section. In the first case, the microgrid is assumed to be operating in grid connected mode. In the second case, the microgrid is assumed to be isolated after sometime and loads are varying after it got isolated. In the third case, the microgrid is assumed to be isolated and generations are assumed to be varying with constant load conditions. In all these cases, the performance of the control strategy in coordinating the control actions of different DGs is examined. The final case study considers relatively severe disturbance in which both grid and PV of the microgrid are disconnected from the remaining part of the considered microgrid.

7.1 Microgrid in grid connected mode

In this case study, the controller is subjected to deliver maximum possible power output from the PV generator and set point power from the DEG. Since the microgrid is operating in grid connected mode, the power that is excess to the load will be supplied to the main grid. The deficiency of power in the microgrid, if any, has to be supplied by the main grid. The solar insolation is assumed to be constant till 3 s and is varying from 50 to 100% in steps, covering 10 to 50% change, during 3 s to 11 s as shown in Fig. 6*a*. Fig. 6*b* depicts the power output of the PV generator for the changing insolations. Since the proposed control philosophy uses the ANN for the V_{dcref} generation and FBLSMC for the control of VSC, the PV generator quickly and accurately tracks the new MPP. The load which consists of an induction motor and impedance is assumed to be constant till 17 s, and beyond which it is assumed to be decreasing as well as increasing as shown in Fig. 6*c*. The DEG set point is changing from 40 to 24 kW at 14 s as shown in Fig. 6*d*. The power that is flowing into the main grid and the system frequency is shown in Figs. 6*e* and *f*, respectively.

In grid connected mode the power that is fed to the grid is nothing but the difference of total power available to the total load in the microgrid. Since the load is assumed to be constant till 17 s, whatever may be the changes in the generation within the microgrid will reflect in the power that is being fed to the main grid as shown in Fig. 6. For example, the solar insolation is assumed to be increased at 3 s, as shown

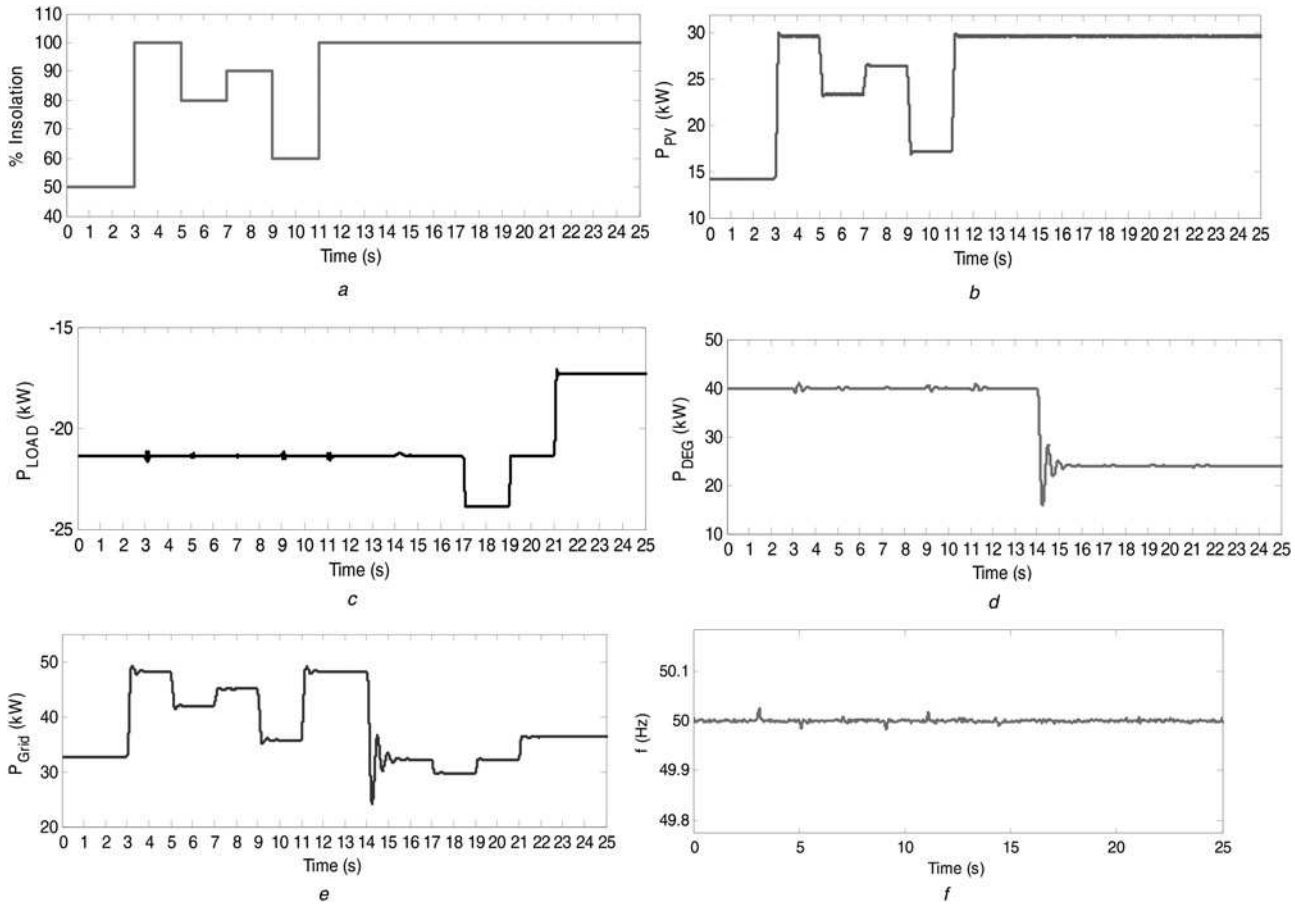

Fig. 6 *Grid connected mode*

a Incident insolation on the PV module
b PV power output
c Load power
d Power generated by DEG
e Power fed to the main grid by microgrid
f Microgrid frequency

doi: 10.1049/iet-gtd.2014.0287

in Fig. 6*a*, hence the PV power output increases to 30 kW (with reference to Fig. 1*b*) as shown in Fig. 6*b*, since the PV is controlled for MPP by the controller. Meanwhile, the DEG set point is constant at 40 kW till 14 s, hence it delivers the same 40 kW as shown in Fig. 6*d*. The load, including the losses, is assumed to be constant at 21 kW till 17 s as shown in Fig. 6*c*. Hence, during 3 to 5 s the total generation in the microgrid is about 70 kW (30 kW + 40 kW) and the total load is 21 kW resulting in excess generation of 49 kW which is fed to the grid as shown in Fig. 6*e*. Since the load and DEG set point is constant till 14 s, for every increase or decrease of insolation, there will be similar increase or decrease in PV power output; hence the difference of power will directly appear in grid feeding as depicted Figs. 6*a*–*e*. Beyond 12 s, the insolation is assumed to be constant till 25 s, hence the PV power output will be constant as depicted in Fig. 6*b*. At 14 s, the DEG set point is assumed to be changing from 40 to 24 kW as shown in Fig. 6*d*. Hence, the total generation in the microgrid falls to 54 kW. Since the load is assumed to be constant till 17 s, the excess power in the microgrid falls to 33 kW, hence the grid feeding decreases to the same amount of 33 kW as shown in Fig. 6*e*. Beyond 14 s, the total available generation is constant at 54 kW till 25 s, however, beyond 17 s there are some load changes (increase as well as decreases) as shown in Fig. 6*c*. Whatever may be the load changes, they will have negative effects in the power that the microgrid is feeding to the main grid, as depicted in Fig. 6*e*. Since the microgrid is operating in grid connected mode, its frequency is constant at 50 Hz as shown in Fig. 6*f*.

7.2 Microgrid transition from grid connected mode to isolated mode and load variations in isolated mode

In this case study, the microgrid is assumed to be isolated from the main grid at 3 s. The load scenario is assumed such that there is excess of generation in the isolated mode so that the efficacy of the proposed control philosophy in maintaining the system stability is analysed in this case study. The performance of the control philosophy in maximum utilisation of available renewable energy without forfeiting the system stability in isolated mode is also evaluated in this case study by considering different load changes.

Since the microgrid got isolated from the main grid at 3 s, the grid feeding is becoming zero (0) from 3 s onwards as depicted in Fig. 7*a*. It can be seen from the Fig. 7*b* that prior to isolation the DEG is delivering same amount (15 KW) of power as that of the case study discussed in Section 3. The solar insolation is assumed to be constant at 100% in this entire case study, hence the maximum power that can be extracted from the PV is 30 kW, as shown in Figs. 6*a* and *b*. The Fig. 7*c* depicts the power that is supplied by the PV generator to the microgrid. The total

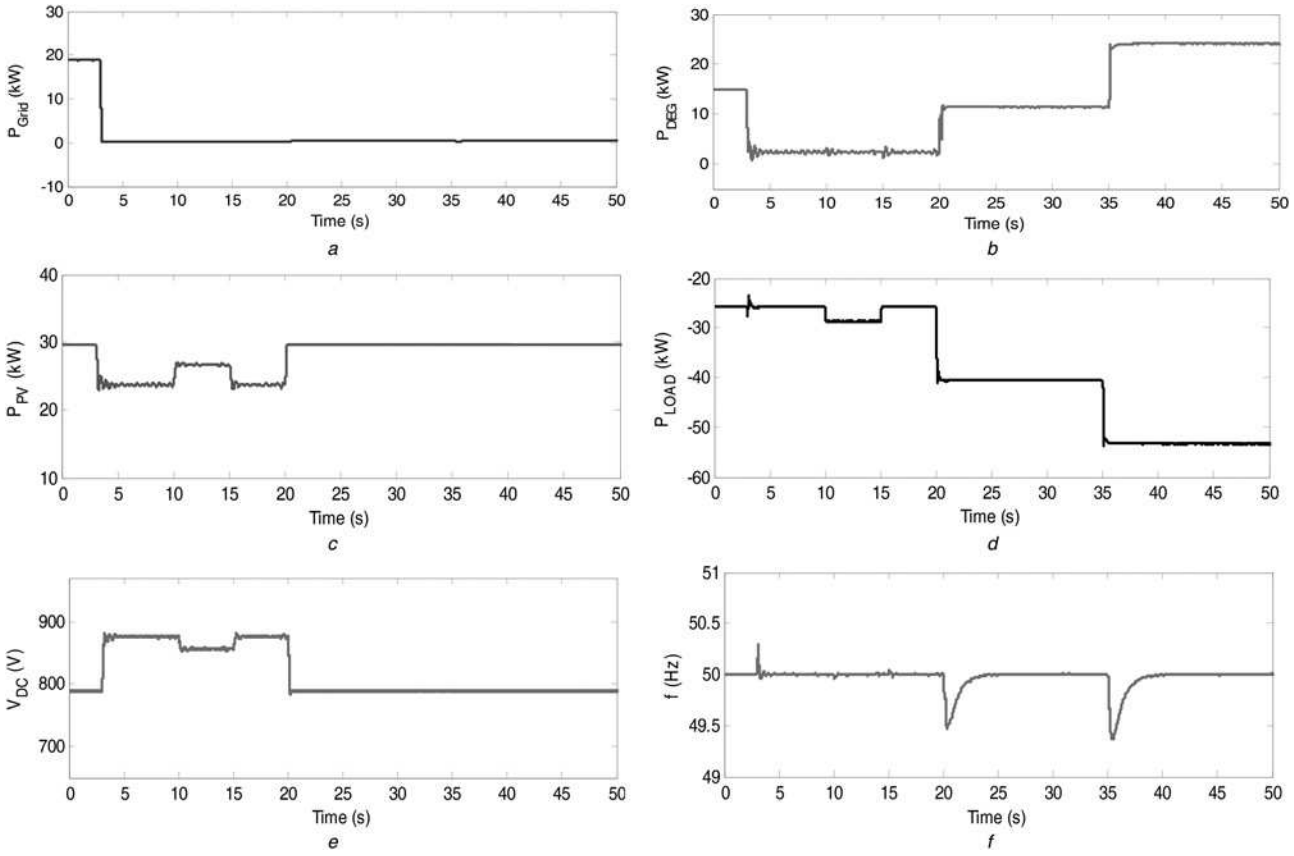

Fig. 7 *Isolated mode with load variations*

a Power fed to the main grid by microgrid
b Power generated by DEG
c PV power output
d Load power
e Operating voltage of the PV module
f Microgrid frequency

load in the microgrid is shown in Fig. 7*d* whereas Fig. 7*e* depicts the operating voltage of the PV module and Fig. 7*f* depicts the microgrid frequency.

Prior to the isolation the total generation in the microgrid is 45 kW (30 kW from PV and 15 kW from DEG) and the total load in the microgrid is only about 26 kW as shown in Figs. 7*b–d*. Hence, till the microgrid gets isolated from the main grid this excess power of about 19 kW will be absorbed by the main grid as depicted in Fig. 7*a*. Once the microgrid gets isolated from the main grid at 3 s, there is excess generation to the tune of 19 kW in the microgrid. With the conventional control philosophies in which the PV is operated at MPP, this excess power will destabilises microgrid as discussed in the Introduction and Section 3. However, with the proposed control philosophy which detects the excess power from the rise of microgrid frequency will make the DEG to deliver minimum output, since the DEG is controlled to deliver only the balance power that cannot be supplied by the PV, as shown in Fig. 1*a*. As the PV is still operating at MPP, the DEG tries to reach its minimum output power, 2.5 kW as shown in Fig. 7*b*. Even though, the DEG is operating at minimum output level, still there is an excess power to the tune of 6.5 kW (2.5 kW + 30 kW – 26 kW). This surplus power can make the microgrid unstable by forcing the DEG to run as motor, if the conventional control methodologies are adopted. However, in the proposed control methodology, this surplus power is reflected in the increase of the frequency, as shown in Fig. 7*f*, and will be detected by the controller. Whenever there is a rise in microgrid frequency, the neuro-fuzzy controller determines the appropriate operating point on the PV characteristic to reduce its output as shown in Figs. 7*c* and *e*, hence to regulate the system frequency and to retain the system stability as shown in Fig. 7*f*. It can be observed from Fig. 7 that, from the instant of isolation, the PV generator has to deliver less power output than the maximum available. Hence, the PV is operated at around 870 V which is higher than its MPP voltage (788 V) to ensure the linear operating region of VSC as shown in Fig. 7*e*.

A typical scenario can be observed from 10 to 15 s, during which the load is increased from 26 to 30 kW as shown in Fig. 7*d*. It can be seen in Fig. 7*b* that the DEG power output undisturbed whereas same amount of power which is equal to the change in the load is increased from the PV generator as shown in Fig. 7*c* by moving the operation towards the MPP, that is, by decreasing the operating voltage as shown in Fig. 7*e*. From this part of the discussion it can be concluded that the proposed controller ensures the maximum utilisation of renewable power without forfeiting the system stability.

The load in the microgrid is increased from 26 to 40 kW at 20 s as shown in Fig. 7*d*. The DEG is delivering 2.5 kW and PV is delivering remaining 23.5 kW as shown in Figs. 7*b–e* till 20 s. Since the load is becoming 40 kW at 20 s, the PV immediately releases its available power and controller instructs it to deliver its maximum possible power to the microgrid. However, the current total generation is only about 32.5 kW (30 kW + 2.5 kW), results in fall of system frequency as shown in Fig. 7*f*. This prompts the DEG is to control its output to balance load, so that DEG increases its output as shown in Fig. 7*b* to regulate the frequency hence to retain the stability. Since the PV is delivering all its available power, for any further increase in the load the DEG regulates its output, hence protects the system from falling into instability as shown in Fig. 7*b–f*. A similar analysis can be carried out for the control phenomenon at 35 s.

Two important observations that can be made from the above Fig. 7 are (i). The proposed control philosophy ensures the maximum possible utilisation of renewable energy. (ii). During the control actions in which PV only responds, the frequency can be brought back into nominal value very quickly (at 5, 10 and 15 s). Whereas the control actions which involve the DEG power regulations, result in delayed process in attaining the nominal frequency. It is because of quick controllability of power electronic converter which is inertia-free, when compared with governor actions which contain some inertia.

7.3 Microgrid transition from grid connected mode to isolated mode and coordinated control of generators for insolation changes

To verify the capability of the controller for bidirectional power flow in a distribution system, that is, active distribution system, the total generation in the microgrid is assumed to be less than the load before the isolation of the microgrid from the main grid. Hence, one can observe the reverse flow of the power from the main grid into the microgrid in Fig. 8*a*. As depicted in Fig. 8*a*, the microgrid is getting isolated from the main grid at 3 s. The solar insolation is assumed to be constant at 30% till first 12 s, hence the PV is delivering 8 kW as its maximum power output as shown in Figs. 8*b* and *c*. Before the microgrid gets isolated from the main grid, the DEG is given with a set point of 32 kW as shown in Fig. 8*d*. Therefore the total generation available in the microgrid prior to isolation is 40 kW (Figs. 8*c* and *d*), where as the total load in the microgrid is about 43 kW including the losses as depicted in Fig. 8*e*. Since, there is a deficiency of 3 kW in the microgrid, the main grid supplies (−3 kW) the microgrid as shown in Fig. 8*a*. Once the microgrid is isolated from the main grid, there is a deficiency of 3 kW in the microgrid which is contrast to the earlier case study. Prior to the isolation, since the PV is operating at MPP, it cannot deliver any extra power to the microgrid even after the isolation as shown in Fig. 8*c*. Therefore the system frequency starts falling from its nominal value as shown in Fig. 8*g*. The fall in the frequency has resulted even after the PV is operating at MPP prompts the controller to activate the governor of the DEG. Hence, because of the governor action the DEG slowly makes-up the deficiency in power to regulate the frequency. During this process the DEG output reaches to 35 from 32 kW. Since the governor is a slow controller when compared with power electronic controllers, and the size of the microgrid is relatively small when compared with the main grid, the fall in the frequency is comparatively high, say 48.5 Hz. Once the DEG compensates for the power deficiency, the microgrid attains its nominal frequency as shown in Fig. 8*g*.

The solar insolation is assumed to be increasing with a slope of 10%/second during 12 to 17 s as depicted in Fig. 8*b*. For these kinds of insolation changes, the controller with P&O based tracker as in [16] will result in unnecessary power oscillations as discussed in Section 4 and degrade the system stability, may force the system to the unstability. Since the solar insolation is increasing and the DEG is operating above its minimum value of 2.5 kW as shown in Figs. 8*b–d*, the controller tries to track the MPP with the help of ANN predictor and FBLSMC which control the VSC of PV generator at MPP as shown in

doi: 10.1049/iet-gtd.2014.0287

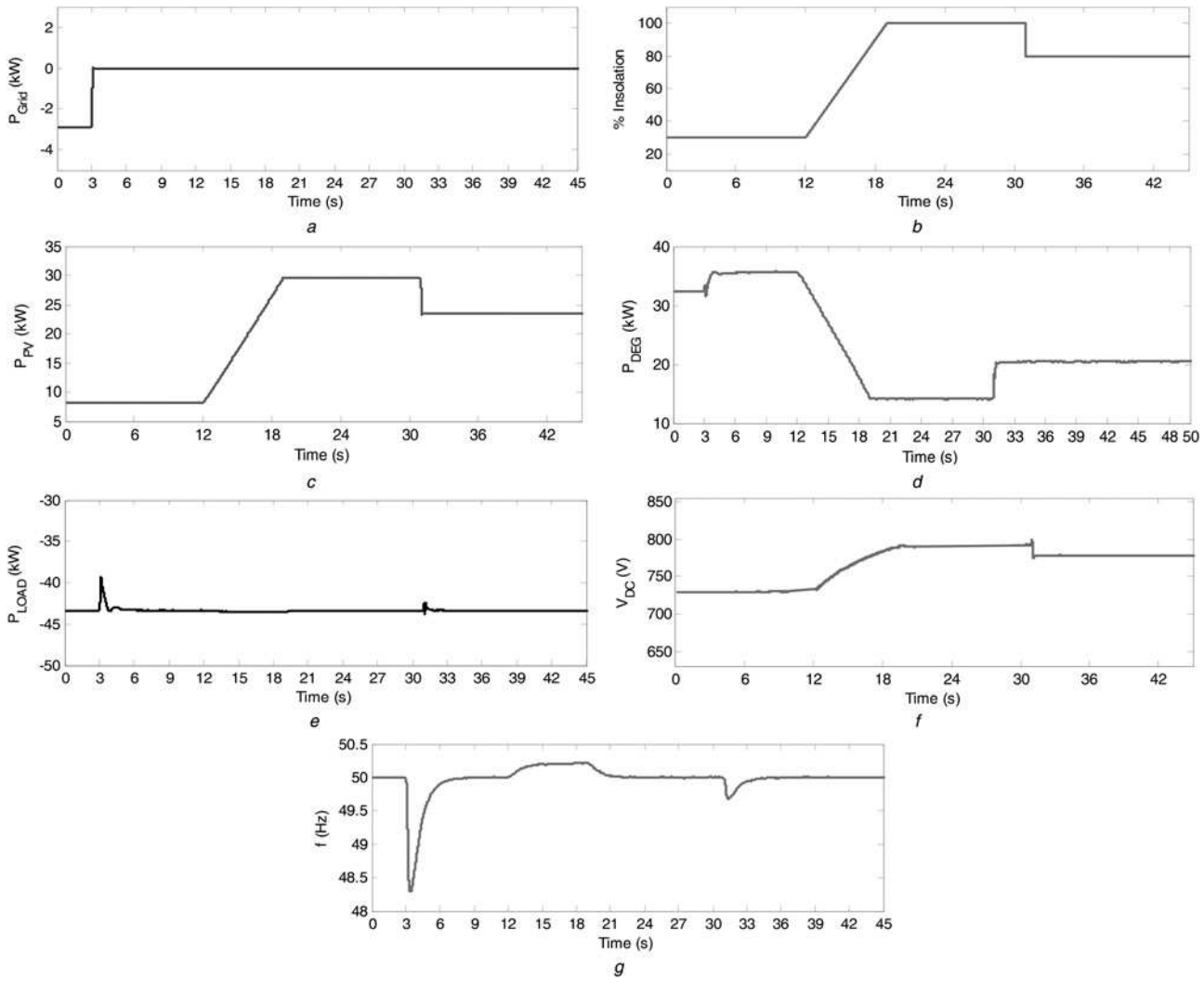

Fig. 8 *Isolated mode with insolation changes*

a Power fed to the main grid by microgrid
b Solar insolation
c PV power output
d Power generated by DEG
e Load power
f Operating voltage of the PV module
g Microgrid frequency

Figs. 8*b*, *c* and *f*. However, the developed neuro-fuzzy controller always keeps on tracking the frequency. In order to avoid unnecessary control actions, the neuro-fuzzy controller is given with a frequency tolerance of 0.2 Hz on the higher side, that is, up to 50.2 Hz. Hence the neuro-fuzzy controller coordinates the control actions of DEG and PV, as and when the frequency hits the upper limit of 50.2 Hz which can be observed from Figs. 8*g*. In this case study, since the PV power output is increasing because of the increase in insolation as shown in Figs. 8*b* and *c*, the neuro-fuzzy controller coordinates the control of DEG so that it decreases its output at the same slope of increase of PV output as shown in Figs. 8*c* and *d*. Once the neuro-fuzzy controller ensures that there no further change in PV power output, it brings back the microgrid frequency to the nominal value as depicted in Fig. 8*g*. For the any decrease of insolation which results in decrease of PV power output will lead to increase in the DEG power output, as shown in Figs. 8*b–d*.

7.4 Microgrid transition from grid connected mode to isolated mode and disconnection of DG at the time of isolation

In this case study, it is assumed that both the PV generator and grid are out at the same instant (3 s) because of fault, forcing the DEG, the only available DG, to stabilise the system and cater the load variations without losing the system stability. The similar load scenario as that of the Section 7.2 is considered here to demonstrate the efficacy of the proposed control philosophy in adapting to the operating conditions. The microgrid is assumed to be isolated from the main grid at 3 s and the PV generator is also disconnected from the microgrid at the same time instant making the disturbance more severe as shown in Figs. 9*a* and *b*. Since the only generator that is available in the microgrid is DEG, it is its sole responsibility to regulate the frequency and stabilise the microgrid. As depicted in Fig. 9*c*, the moment when the microgrid is isolated from the main grid, frequency starts

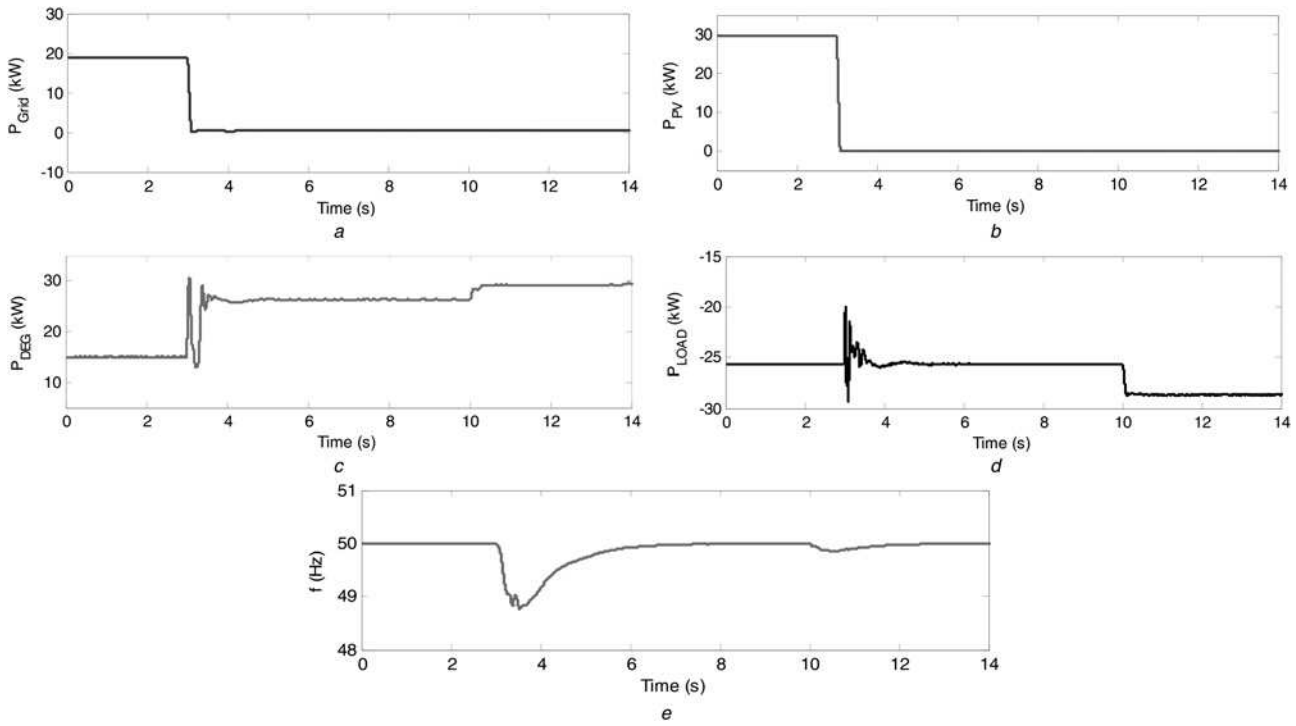

Fig. 9 *Grid isolation and PV disconnection*

a Power fed to the main grid by microgrid
b PV power output
c Power generated by DEG
d Load Power
e Microgrid frequency

decreasing. Since the PV generator output also became zero, the DEG starts responding to the frequency deviation and stabilises the system as shown in Figs. 9*c* and *e*. For the load increase at 10 s, the DEG increases its power output accordingly and maintains the system stability as shown in Figs. 9*c* and *d*. From this case study, it can be concluded that the proposed control philosophy can accommodate different disturbances and can effectively adapt to the various operating conditions.

8 Performance comparison of fuzzy and PI controllers

A case study discussed in Section 7.2 is re-considered here to compare the performances of the proposed fuzzy and conventional PI [16] controllers in stabilising the frequency excursion of the microgrid. The performance is examined by replacing the fuzzy controller with PI controller, however, the limiting voltages are generated with the help

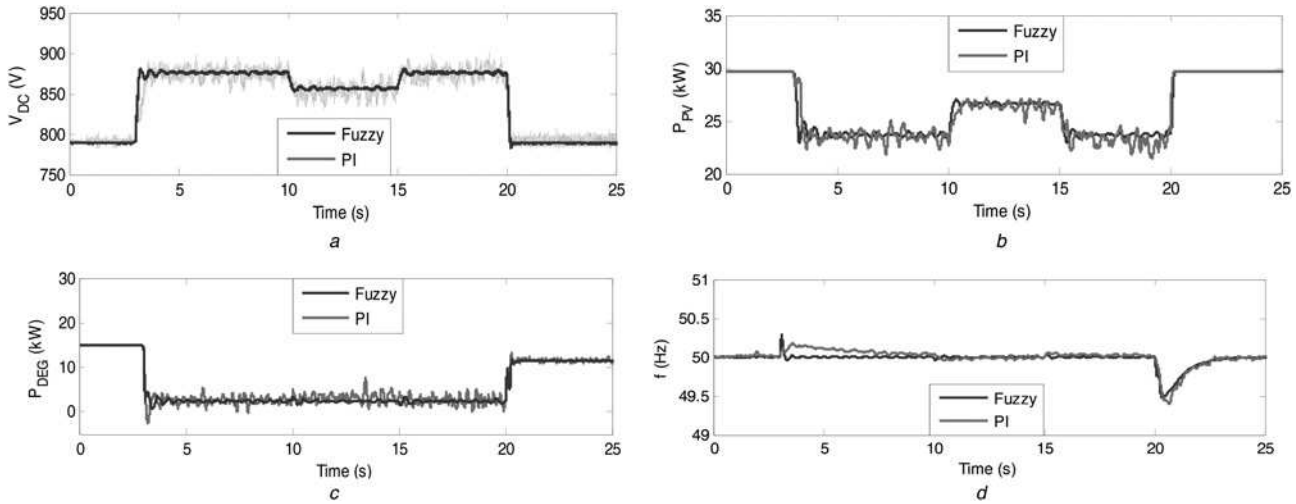

Fig. 10 *Proposed fuzzy against PI*

a Operating voltage of the PV module
b PV power output
c Power generated by DEG
d Microgrid frequency

doi: 10.1049/iet-gtd.2014.0287

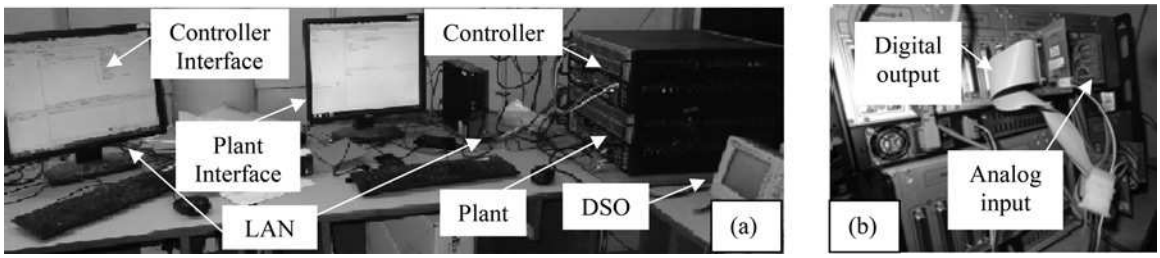

Fig. 11 *Validation in real-time environment*

a Implementation in real-time environment using OPAL-RT's OP5600s
b Connections at the rear end

of ANN based adaptive-predictor-corrector as discussed earlier. Fig. 10 depicts the system responses with the fuzzy as well as PI controllers. In any case, maintaining the system stability is the prime objective. Hence, the PI controller is tuned ($K_{p\text{Deload}}$, $K_{i\text{Deload}}$) such that the system frequency is regulated as quickly as possible so as to maintain the system stability.

As depicted in Fig. 10 both the fuzzy and PI controller are able to stabilise the system during the transition from grid connected mode to isolation mode (3 s). In addition, both the controllers are able to regulate the frequency for different load changes as shown in Fig. 10*d*. PI controller is delivering comparable frequency regulation performance, on par with the fuzzy controller, for the disturbances at 10 s and 15 s. However, for the disturbance at 3 s (isolation of microgrid from grid), PI controller is delivering sluggish response as shown in Fig. 10*d*. In addition, the PI controller is also resulting in motoring operation of DEG for short duration at 3 s, as shown in Fig. 10*c*, which is not good from the point of view of DEG ageing, wear and tear. The PI response is quite oscillatory which further increases the wear and tear of the DEG. In contrast, the fuzzy controller is able adapt its gain and delivering superior performance by not allowing the DEG to enter the motoring operation, quickly regulating the frequency for all the disturbances considered and oscillation free response in steady state with minimum oscillations during transients.

9 Validation of proposed control philosophy in real-time environment

The proposed control scheme is validated in the real-time environment using two OP5600 systems of OPAL-RT as shown in Fig. 11*a*. To realise the complete microgrid system, one of the OP5600 systems is made to work as controller where as the other OP5600 will work as plant which includes all the generators and loads along with the main grid. The controller system will receive analog signals from the plant system and generates necessary control actions based on the proposed control philosophy. These control actions in the form of digital signals will be communicated to the plant OP5600 as shown in Fig. 11*b*. Therefore, the communication between the two OP5600 systems which are working individually as plant and controller is carried out externally, hence realising a hardware-in-loop (HIL) system. The performance of the proposed control scheme is examined by recording the various responses using digital storage oscilloscope (DSO).

The following Fig. 12 depicts the system performance under grid isolation with conventional control scheme, as discussed in Section 3. From Fig. 12, it can be confirmed that the conventional control philosophies, which operate the PV generator at MPP all the time, can make the microgrid unstable once it got isolated from the main grid, as concluded in Section 3.

The system performance in grid connected mode under different generation and load changes, as discussed in Section 7.1 is depicted in Fig. 13. The same generation changes (insolation changes for PV and mechanical input changes for DEG) and load changes as that of the Section 7.1 are considered here as well, to validate the system performance in real-time environment. As concluded in Section 7.1, the generation changes are having positive impact (grid feeding increases with the increase in generation for constant load) whereas the load change has negative impact on the grid feeding. The results obtained in real-time environment are completely complying with the results obtained through numerical simulations.

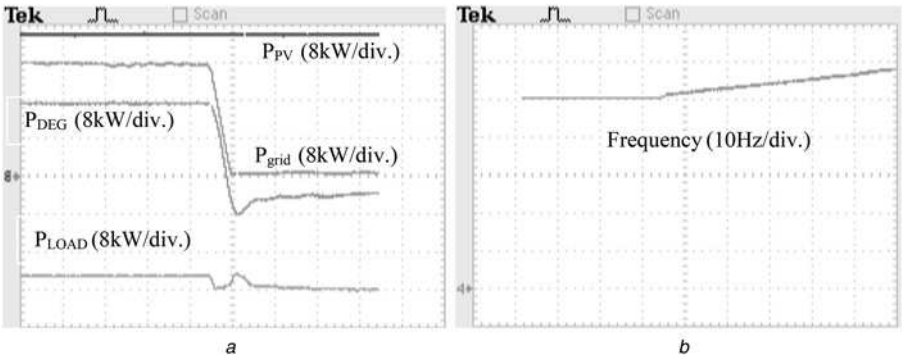

Fig. 12 *Case study-1*

a Power outputs of different devices with conventional control philosophy
b Microgrid frequency

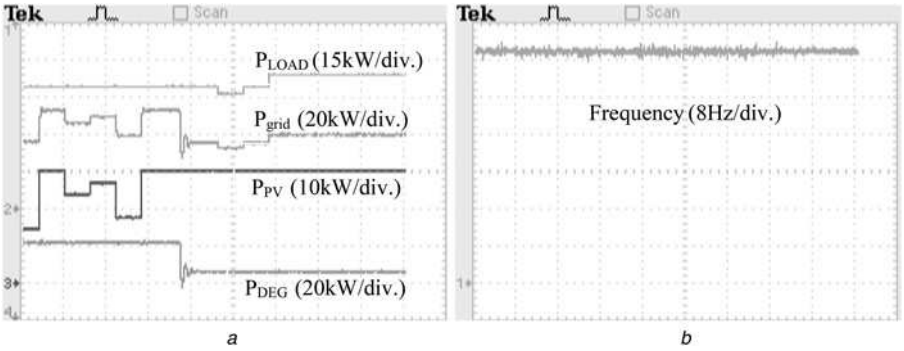

Fig. 13 *Case study-2*

a Power outputs of different devices in grid connected mode
b Microgrid frequency

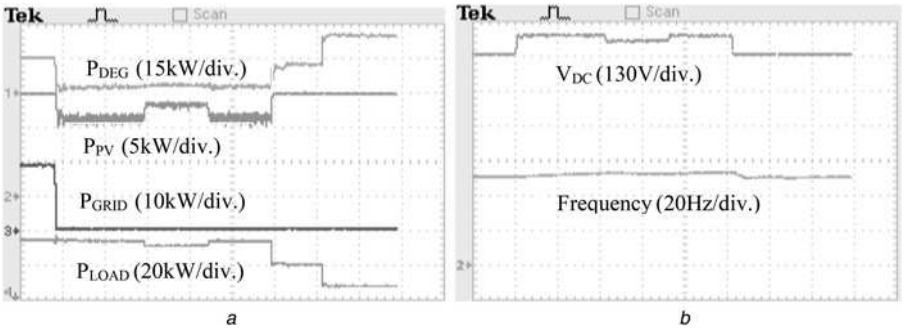

Fig. 14 *Case study-3*

a Power outputs of different devices during, before and after the transition of microgrid from grid connected mode to off-grid mode
b DC link voltage of PV generator and Microgrid frequency

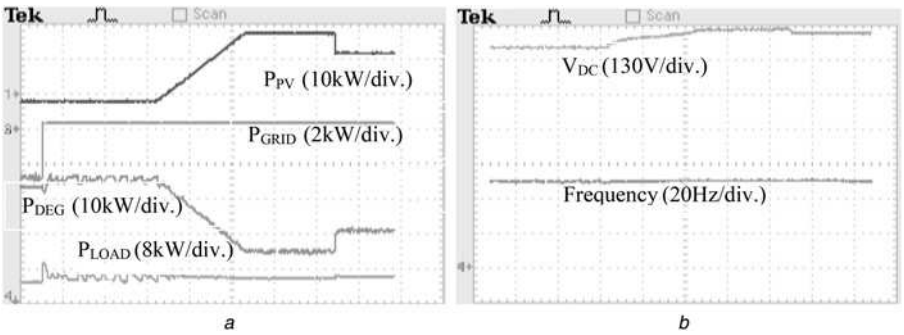

Fig. 15 *Case study-4*

a Power outputs of different devices during, before and after the transition of microgrid from grid connected mode to off-grid mode for different insolation changes
b DC link voltage of PV generator and Microgrid frequency

Fig. 14 illustrates the performance of the proposed controller under grid isolation with different load changes as discussed in Section 7.2. Power outputs of different devices are shown in Fig. 14*a* where as Fig. 14*b* depicts the microgrid frequency and dc link voltage of PV generator before, during and after the trasistion of microgrid from grid connection mode to isolated mode. The microgrid is being isolated at 3 s (at first time division in Fig. 14) resulting in excess power in the microgrid than its load. With the conventional control philosophies, the system becomes unstable as depicted in Figs. 2 and 12. However, with the proposed control philosophy the PV is derated in cordination with the DEG to maintain the system frequency and hence its stability. These results are completely complying with the numerical simulation results presented in Section 7.2.

The performance validation of the control philosophy for secnario discussed in Section 7.3 in real-time environment is illustrated in Fig. 15. As concluded in the Section 7.3, the proposed control philoopshy is able to stabilise the system with proper coordination of DEG output by ensuring maximum possible utilisation of available PV power for different insolation changes.

10 Conclusions

A novel neuro-fuzzy controller based on data analytics is proposed in this paper to ensure stable operation of

doi: 10.1049/iet-gtd.2014.0287

DEG-PV hybrid AC microgrid in both grid connected and isolated modes. In grid connected mode, the proposed controller operates the PV at MPP and DEG at it desired set points. In isolated mode the proposed controller keeps on tracking the microgrid frequency and co-ordinately controls the both DEG and PV to assure the system stability. Besides, the proposed control philosophy utilises the available PV power to the best by saving the fuel of DEG. The efficacy of the proposed neuro-fuzzy controller is evaluated under different operating conditions and is rendering very good performance. The performance of the proposed control philosophy is validated in real-time environment.

11 Acknowledgment

This work was supported in part by DST, Government of India under its project 'Developments of robust controller for seamless operation of microgrid.' File No:SB/S3/EECE/0122/2013.

12 References

1 Venayagamoorthy, G.K., Rohrig, K., Erlich, I.: 'One step ahead: short-term wind power forecasting and intelligent predictive control based on data analytics', *IEEE Power Energy Mag.*, 2012, **10**, pp. 70–78
2 Katiraei, F., Iravani, M.R.: 'Power management strategies for a microgrid with multiple distributed generation units', *IEEE Trans. Power Syst.*, 2006, **21**, (4), pp. 1821–1831
3 Khanh, L.N., Seo, J.-J., Kim, Y.-S., Won, D.-J.: 'Power-management strategies for a grid-connected PV-FC hybrid system', *IEEE Trans. Power Deliv.*, 2010, **25**, pp. 1874–1882
4 Datta, M., Senjyu, T., Toshihisa Funabashi, A.Y., Kim, C-H.: 'A frequency-control approach by photovoltaic generator in a PV–diesel hybrid power system', *IEEE Trans. Energy Convers.*, 2011, **26**, pp. 559–571
5 Subudhi, B., Pradhan, R.: 'A comparative study on maximum power pointtracking techniques for photovoltaic power systems', *IEEE Trans. Sustain. Energy*, 2013, **4**, pp. 89–98
6 Muljadi, E., Mckenna, H.E.: 'Power quality issues in a hybrid power system', *IEEE Trans. Ind. Appl.*, 2002, **38**, pp. 803–809
7 Elmitwally, A., Rashed, M.: 'Flexible operation strategy for an isolated PV-diesel microgrid without energy storage', *IEEE Trans. Energy Convers.*, 2011, **26**, pp. 235–244
8 Bhende, C.N.: 'Stand-alone wind energy supply system'. Third Int. Conf. on Power Systems, Kharagpur, 2009, December 27–29
9 Lee, D-J., Wang, L.: 'Small-signal stability analysis of an autonomous hybrid renewable energy power generation/energy storage system part I: time-domain simulations', *IEEE Trans. Energy Convers.*, 2008, **23**, pp. 311–320
10 Bevrani, H., Habibi, F., Babahajyani, P., Watanabe, M., Mitani, Y.: 'Intelligent frequency control in an AC microgrid: online PSO-based fuzzy tuning approach', *IEEE Trans. Smart Grid*, 2012, **3**, pp. 1935–1944
11 Dufo-Ĺopez, R., Bernal, J.L.: 'Design and control strategies of PVdiesel systems using genetic algorithms', *Solar Energy J.*, 2005, **79**, pp. 33–46
12 Wakao, S., Nakao, K.: 'Reduction of fuel consumption in PV/diesel hybrid power generation system by dynamic programming combined with genetic algorithm'. Proc. Conf. Record IEEE Fourth World Conf. Photovoltaic Energy Conversion, May 2006, vol. 2, pp. 2335–2338
13 Abdin, E.S., Osheiba, A.M., Khater, M.M.: 'Modeling and optimal controllers design for a stand-alone photovoltaic-diesel generator unit', *IEEE Trans. Energy Convers.*, 1999, **14**, pp. 560–565
14 Argaw, N., Foster, R., Ellis, A.: 'Renewable energy for water pumping applications in rural villages', Report No. NREL/SR-500-30361, National Renewable Energy Lab., Golden, CO, Jul. 2003
15 Rahman, M., Osheiba, A., Radwan, T., Abdin, E.: 'Modelling and controller design of an isolated diesel engine permanent magnet synchronous generator', *IEEE Trans. Energy Convers.*, 1996, **11**, pp. 324–330
16 Mishra, S., Ramasubramanian, D., Sekhar, P.C.: 'A seamless control methodology for a grid connected and isolated PV-diesel microgrid', *IEEE Trans. Power Syst.*, 2013, **28**, pp. 4393–4404
17 Mishra, S., Dash, P.K., Panda, G.: 'TS-fuzzy controller for UPFC in a multimachine power system', *Proc, Inst. Electr. Eng., Gen., Trans. Distrib.*, 2000, **174**, pp. 15–22
18 Wasynczuk, O.: 'Modeling and dynamic performance of a line commutated photovoltaic inverter system', *IEEE Trans. Energy Convers*, 1989, **4**, pp. 337–343
19 Messenger, R., Ventre, J.: 'Photovoltaic systems engineering' (CRC Press, 2000), pp. 41–51
20 Mishra, S., Sekhar, P.C.: 'TS fuzzy implications based novel adaptive perturb MPPT algorithm for grid connected single stage three phase VSC interfaced photovoltaic generating system', IEEE PES General Meeting, 2012
21 Carrasco, J.M., Franquelo, L.G., Bialasiewicz, J.T., *et al.*: 'Power-electronic systems for the grid integration of renewable energy sources: a survey', *IEEE Trans. Ind. Electron.*, 2006, **53**, pp. 1002–1016
22 Kerekes, T., Teodorescu, R., Liserre, M., Klumpner, C., Sumner, M.: 'Evaluation of three-phase transformerless photovoltaic inverter topologies', *IEEE Trans. Power Electron.*, 2009, **24**, pp. 2202–2211
23 Mishra, M.K., Karthikeyan, K.: 'A fast-acting DC-link voltage controller for three-phase DSTATCOM to compensate AC and DC loads', *IEEE Trans. Power Deliv.*, 2009, **24**, pp. 2291–2299
24 Gaztañaga, H., Etxeberria-Otadui, I., Ocnasu, D., Bacha, S.: 'Real-time analysis of the transient response improvement of fixed-speed wind farms by using a reduced-scale STATCOM prototype', *IEEE Trans. Power Syst.*, 2007, **22**, pp. 658–666
25 Blaabjerg, F., Teodorescu, R., Liserre, M., Timbus, A.V.: 'Overview of control and grid synchronization for distributed power generation systems', *IEEE Trans. Ind. Electron.*, 2006, **53**, pp. 1398–1409
26 Moni, R.S., Mahimkar, N., Persson, G.: 'VSC Converter Systems to Enhance Grid Stability and Ensure Reliable Power to Cities'. GridTech, New Delhi, India, Apr. 2013, pp. 1–6
27 Samangkool, K., Premrudeepreechacharn, S.: 'Maximum power point tracking using neural networks for grid-connected photovoltaic system'. Int. Conf. on Future Power Systems, Amsterdam, Nov. 2005, pp. 1–4
28 Sekhar, P.C., Mishra, S.: 'Sliding mode based feedback linearizing controller for grid connected multiple fuel cells scenario', *Int. J. Electr. Power Energy Syst.*, 2014, **60**, pp. 190–202

13 Appendix

13.1 Parameters of the PV module

$N_p = 5$, $N_s = 1050$, $I_{SC} = 8.03\text{A}$, $I_{rs} = 1.2 \times 10^{-7}\text{A}$, $q = 1.602 \times 10^{-19}\text{C}$, $k = 1.38 \times 10^{-23}\text{J/K}$, $A = 1.92$, $T_{\text{ref}} = 300°\text{K}$, $K_I = 0.0017$

13.2 Controller parameters

$\dot{\Delta f}_1 = -10$, $\dot{\Delta f}_2 = -10$, $\dot{\Delta f}_3 = -5$, $\dot{\Delta f}_4 = -5$, $\dot{\Delta f}_5 = -3$, $\dot{\Delta f}_6 = 0$, $\dot{\Delta f}_7 = 0$, $\dot{\Delta f}_8 = 0$, $\dot{\Delta f}_9 = 3$, $\dot{\Delta f}_{10} = 5$, $\dot{\Delta f}_{11} = 5$, $\dot{\Delta f}_{12} = 10$, $\dot{\Delta f}_{13} = 10$, $\Delta f_1 = -1$, $\Delta f_2 = -0.25$, $\Delta f_3 = -1$, $\Delta f_4 = -0.2$, $\Delta f_5 = -0.25$, $\Delta f_6 = 0$, $\Delta f_7 = 0$, $\Delta f_8 = 0$, $\Delta f_9 = 0.25$, $\Delta f_{10} = 0.25$, $\Delta f_{11} = 0.25$, $\Delta f_{13} = 1$, $\Delta f_{13} = 1$, $K_{p\text{DEG}} = 0.2$, $K_{i\text{DEG}} = 0.09$, $K_{p\text{Deload}} = -400$; $K_{i\text{Deload}} = -100$.